DOE/ET-53088-230 IFSR #230

Resistive Fluid Turbulence in Diverted Tokamaks and the Edge Transport Barrier in *H*-mode Plasmas

T. S. Hahm and *P. H. Diamond*

Institute for Fusion Studies
The University of Texas at Austin
Austin, Texas 78712-1060

July 1986

Resistive Fluid Turbulence in Diverted Tokamaks and the Edge Transport Barrier in H-mode Plasmas

T. S. Hahm and *P. H. Diamond*
Institute for Fusion Studies
The University of Texas at Austin
Austin, Texas 78712-1060

Abstract

The thermal and particle diffusivities driven by resistive fluid turbulence in diverted tokamak edge plasmas are calculated. Diverted tokamak geometry is characterized by increased global shear near the separatrix and the tendency of field lines to linger near the x-point. For resistive fluid turbulence, the dominant effect is increased global shear, which causes a reduction in the effective step-size of the turbulent diffusion process and corresponding improvements in heat and particle confinement close to the separatrix. Stability of resistive kink modes resonant near separatrix is also ensured by the increased global shear. The relevance of these considerations to the $L \rightarrow H$ transition and to the edge transport barrier in H-mode plasmas is discussed.

I. Introduction

Degradation of particle and energy confinement during auxiliary heating (L-phase) of tokamak plasmas is an almost universal experimental observation. An exception to this trend is the H-mode confinement regime, first discovered on the ASDEX tokamak[1] and subsequently observed in other diverted tokamak experiments.[2-4] The H-mode operation is characterized by improved energy and particle confinement, with τ_E and τ_P (the energy and particle confinement times, respectively) comparable in magnitude to, but scaling differently than, values for corresponding ohmically heated plasmas.

It has been observed that a critical minimum heating power (1.2 MW on ASDEX) is required for a transition to H-mode operation.[5] For slightly subcritical heating powers, the transition can be triggered by the arrival of a sawtooth-crash-induced heat pulse at the plasma periphery. At the H-mode transition, an edge transport barrier forms in the vicinity of the separatrix. This transport barrier is located in a region within approximately 4 cm. of the separatrix, where global shear increases dramatically. The H-mode plasmas are thus characterized by high edge temperatures, very steep edge density and temperature gradients ($T_e \approx 450$eV, $L_n \approx 4$ cm, $L_T \approx 3$ cm at 2 cm from separatrix), and good particle confinement. Temperature profile broadening, so that $q(0) > 1$ (no sawteeth in H-mode!), and a global reduction of the thermal diffusivity $\chi_e(r)$ follow the formation of the edge transport barrier.[6] Finally, on ASDEX where $a = 40$ cm, the thermal diffusivity deduced from transport simulations[7] of H-mode discharges peaks and begins to decrease with increasing radius for $r > 32$cm.

The apparent necessity of a divertor for formation of the edge transport barrier and the ensuing transition to H-mode naturally motivates questions related to the effects of separatrix geometry and high edge temperatures on edge turbulence and to the stability of H-mode plasma profiles. Alternatively, what aspects of separatrix geometry facilitate the apparent transition of the edge plasma from a turbulent state of poor confinement to a relatively quiescent state of good confinement with significantly different profile? However, in order to address such questions, some insight into the physical mechanisms which govern the ambient edge turbulence during *ohmic* heating and *L-phase* operation is necessary. While results from various studies differ in detail, edge turbulence in ohmic

plasmas is generally characterized by:

i) large density and potential fluctuations,[8-12] i.e., $\tilde{n}/n > .2$, $e\hat{\phi}/T_e > .3$

ii) $\tilde{n}/n \neq e\hat{\phi}/T_e$, i.e., breakdown of the Boltzmann relation[11]

iii) broad frequency spectra and large radial correlation lengths, i.e., $\Delta\omega \sim \omega$ and $\Delta r_c \sim 1$ cm, where typically the effective ion Larmor radius $\rho_s \sim .02$ cm.

iv) density fluctuation levels which decrease with increasing plasma current[13]

v) particle and heat transport which are dominated by convection, with particle diffusivity $D_n \sim 10^4 - 10^5 cm^2/\text{sec}$

vi) a favorable scaling of τ_P with current and an unfavorable scaling with toroidal field.[14]

Edge turbulence in L-phase plasmas is characterized by:

i) the persistence of the ambient electrostatic edge turbulence, with increased fluctuation levels[12]

ii) the appearance of broadband, high frequency, i.e., $\omega \sim$ 100kHz magnetic fluctuations,[3,5,15-18] with fluctuation levels increasing with poloidal beta β_p [15] or, alternatively, injection power

iii) an increased sensitivity of magnetic fluctuations to off-axis power deposition[17]

iv) a decrease in the confinement time of runaway electrons, which accompanies degraded energy and particle confinement.[18]

Edge plasmas during H-mode are characterized by:

i) *increased* runaway confinement times, in comparison to L-mode[16]

ii) improved particle confinement, as indicated by an abrupt reduction in H_α emission

iii) broad profiles, with very steep density and temperature gradients near the edge.

These three sets of observations, along with those pertinent to the $L \rightarrow H$ transition already discussed above, suggest that the ambient plasma edge turbulence is likely

to be resistive fluid turbulence, rather than drift wave turbulence, with an electromagnetic component which increases rapidly with β_p. This suggestion is consistent with ASDEX edge plasma parameters, which indicate that $\nu_{*e} \gtrsim 2$ and $S_m \lesssim 10^6$ during L-phase. Two concrete, relevant paradigms for resistive fluid turbulence are resistive pressure gradient-driven turbulence[15] and resistivity gradient-driven turbulence,[19,20] respectively. Resistive pressure gradient-driven turbulence, which evolves from resistive ballooning modes, drives radially-localized magnetic perturbations which increase with β_p according to $\tilde{B}_\theta/B_\theta \sim \beta_p^{7/6}$, and which cause thermal transport, with diffusivity $\chi_e \cong \frac{3}{2} v_{te} a \frac{q}{S_m} \left(\alpha/\hat{s}\right)^{3/2}$. Resistivity gradient driven turbulence,[19,20] which evolves from rippling modes, is driven by temperature and impurity density gradients and causes particle transport with diffusivity D_n. The magnitude and parameter scalings of D_n are consistent with results from several studies of tokamak edge turbulence and particle transport. Thus, resistive pressure gradient driven turbulence and resistivity gradient driven turbulence are good *resistive fluid model paradigms* for an electromagnetic, thermal transport mechanism and an electrostatic particle transport mechanism, respectively.

In this paper, the effects of separatrix geometry on thermal and particle transport triggered by resistive pressure gradient driven turbulence and resistivity gradient driven turbulence are investigated. There are two principal modifications to available theoretical predictions introduced by separatrix geometry. First, since B_p, the poloidal magnetic field, tends to vanish at x-points of the separatrix, the safety factor $q_{\rm MHD}$ diverges as $\rho \rightarrow 1$ for fixed q_c (the safety factor obtained for circular flux surfaces), where ρ is the normalized radial coordinate ($\rho = 1$ corresponds to separatrix), i.e.,

$$\begin{aligned} q_{\rm MHD}(r) &= \frac{1}{2\pi} \oint \frac{d\ell}{R_0} \frac{B_\phi}{B_p} \\ &= q_c \frac{2}{\pi} \mathbf{K}(\rho) \sim q_c \frac{2}{\pi} \ln\left(4/\sqrt{1-\rho^2}\right), \quad \rho \rightarrow 1 \end{aligned}$$

for model equilibrium employed in Sec. II. Consequently, parallel length scales such as the connection length $L_c = R q_{\rm MHD}$ and the parallel correlation length $L_{\|} = R q_{\rm MHD} \Delta\ell / r_0$, where $\Delta\ell$ is the mode extent in the *extended* poloidal coordinate, also diverge. Second,

the global shear $\hat{s} = d\ln q_{\rm MHD}/d\ln\rho$ also diverges as $\rho \to 1$, i.e.,

$$\begin{aligned}\hat{s} &= d\ln q_{\rm MHD}/d\ln\rho \\ &= \hat{s}_{\rm cyl} + \frac{\mathbf{E}(\rho)}{\mathbf{K}(\rho)(1-\rho^2)} - 1 \sim 1/(1-\rho^2)\ln\left(1/\sqrt{1-\rho^2}\right), \quad \rho \to 1.\end{aligned}$$

Thus, radial scale lengths such as the layer width (radial correlation length) $\Delta r \sim r_0/k_\theta \hat{s}\Delta\ell$ shrink as $\rho \to 1$. It is important to note that $\lim_{\rho\to 1}\hat{s}(\rho)$ diverges algebraically while $\lim_{\rho\to 1} q_{\rm MHD}(\rho)$ diverges logarithmically. Therefore, since resistive fluid turbulence is driven by resonant fluctuations which already extend along the magnetic field lines ($\Delta\ell \gg 2\pi r_0$) with small radial scale lengths $\Delta r \sim r_0/k_\theta\hat{s}\Delta\ell$, the principal effect of separatrix geometry is a reduction in the characteristic radial scale length Δr due to increased global shear. It follows that thermal and particle diffusivities vanish algebraically as $\rho \to 1$, consistent with the notion of a transport barrier.[5] In particular, for the model separatrix geometry considered here, significant reduction of χ_E and D_n occurs for $\rho > .9$, while departure from the circular-flux-surface model begins at $\rho \sim .8$. For ASDEX, $a = 40$ cm. so that these radii correspond to $r = 36$ cm. and $r = 32$ cm., respectively. These predictions are in reasonable agreement with the results of transport analyses.[7] Also, stability of resistive kink modes resonant near the separatrix is shown to follow from the increased values of $q_{\rm MHD}$ and global shear characteristic of that region. Thus, separatrix geometry can support the large plasma current gradients characteristic of H-mode.

Previous investigations of the effects of separatrix geometry on instabilities have focused on the ideal ballooning mode. In particular, in Ref. 21, it was noted that field line lingering near the (separatrix) x-point rather than increased global shear controls ideal ballooning stability near the separatrix. Thus, the poloidal location of the x-point plays an important role in ideal ballooning stability. For the divertor configuration of ASDEX where x-point is located at the top or bottom of the torus, the conclusion of Ref. 21 was that separatrix geometry had little effect on ideal ballooning instabilities. This conclusion appears to be in accord with experimental results which indicate that the non-disruptive β limit, which is reached *after* the $L \to H$ transition occurs, is reasonably consistent with expectations based on simple ideal ballooning stability considerations.[22] This observation, together with the fact that the $L \to H$ transition occurs for quite modest β, suggests that

ideal ballooning stability does not *uniquely* govern H-mode confinement. It is instructive to note that in contrast to ideal modes, resistive instabilities require decoupling of fluid and magnetic field dynamics by dissipation near $\vec{k}\cdot\vec{B}_0 = 0$ resonances. Hence, long parallel scales are intrinsic to resistive modes, which consequently do not tend to "linger" like ideal modes do. Thus, it is not surprising that increased global shear has a greater impact on resistive fluid turbulence. Finally, it should be noted that while certain specific models are discussed in detail here, the conclusions are quite generic and apply to *any* resistive fluid turbulence model.

The principal results of this paper are:

i) the thermal and particle diffusivities corresponding to resistive pressure gradient driven and resistivity gradient driven turbulence are calculated for separatrix geometry.

ii) the principal effect of separatrix geometry on resistive fluid turbulence is a decrease in the characteristic radial scale length (step size) due to increased global shear.

iii) resistive kink stability of modes resonant near the separatrix is also shown to follow from the increased values of global shear and safety factor characteristic of that region.

iv) the reduced radial scale length results in reduced χ_E and D_n near the separatrix ($\rho > .9$), consistent with the notion of a transport barrier. In addition, reduced Δr results in reduced magnetic fluctuation levels, consistent with good runaway confinement in H-mode.

v) for ASDEX, the zone of improved confinement is predicted to be localized to $r > 36$cm, with departure of $\chi_E(r)$ from its circular-flux-surface analogue beginning at $r = 32$ cm. These predictions are in reasonable agreement with the results of transport analyses.[7]

vi) two scenarios related to the $L \rightarrow H$ transition are proposed. These are based on the dynamics of resistive fluid turbulence, and depend on the interplay of various physical processes discussed in this paper.

The remainder of this paper is organized as follows. The separatrix-geometry model

equilibrium is described in Sec. II. In Sec. III, the linear stability conditions for resistive kink modes resonant near the edge of diverted tokamaks are presented. In Sec. IV, the linear theory of resistive ballooning modes in separatrix geometry is presented. Saturated resistive pressure gradient driven fluid turbulence and the associated anomalous electron thermal conductivity are discussed in Sec. V. Particle transport in diverted tokamak edge plasmas resulting from resistivity gradient driven turbulence model is discussed in Sec. VI. In Sec. VII, several scenarios related to the $L \rightarrow H$ transition are discussed.

II. Separatrix-Geometry Equilibrium

In this section, a model separatrix geometry (divertor) equilibrium is described and the relevant equilibrium quantities are calculated. To simplify analytical calculation, we consider a 2-null model equilibrium adopted by Qu and Callen[23] for use in an ideal ballooning mode stability analysis. Although this model equilibrium is obviously an over-simplification of the real situation, we expect to explore the general features of the resistive modes and turbulence within this model. The most interesting property of the divertor geometry is one which this model successfully simulates, namely that the poloidal magnetic field vanishes at the stagnation points. Other model-specific features, for example the detailed shape of the flux surfaces, do not change the basic conclusions of this work. The equilibrium magnetic field is given by

$$\vec{B} = B_\phi R_0 \nabla\zeta + \nabla\zeta \times \nabla\psi.$$

Here, ψ is the poloidal flux function given by

$$\psi = R_0 B_\phi \left(\frac{x^2}{2L_q} - \frac{\delta}{\kappa} \cos\kappa y \right), \tag{1}$$

where x, y are cartesian coordinates in a ζ (toroidal angle) = constant cross section, B_ϕ is the toroidal magnetic field, which is assumed to be uniform throughout this paper. From Eq. (1), magnetic flux surfaces (where ψ = const) are described by

$$x^2 + x_s^2 \sin^2\left(\frac{\kappa y}{2}\right) = x_0^2, \tag{2}$$

where $x_s^2 = 4\delta L_q/\kappa$, and $x_0^2 = 2L_q\left(\frac{\psi}{R_0 B_\phi} + \frac{\delta}{\kappa}\right)$. Hence, a sequence of magnetic flux surfaces with different shape can be parametrized by a dimensionless quantity $\rho \equiv x_0/x_s$

(see Fig. 1). Also, in order to facilitate direct comparisons with circular-flux-surface results, we choose $\kappa x_s = 2$. Hence, $x^2 + y^2 = x_0^2$, as $\rho \to 0$, and the $\rho = 1$ surface corresponds to the separatrix. The magnitude of the poloidal magnetic field is given by

$$B_p^2 = B_\phi^2 \left\{ \left(\frac{x}{L_q} \right)^2 + \delta^2 \sin^2 \kappa y \right\}. \tag{3}$$

At x-points, where $x = 0$, $y = \pm \frac{\pi}{\kappa}$, the poloidal magnetic field vanishes.

The equilibrium quantities of interest are the safety factor q_{MHD} and the global shear $\hat{s}$. The safety factor is defined by

$$q_{\text{MHD}} = \frac{1}{2\pi} \oint \frac{d\ell}{R_0} \frac{B_\phi}{B_p},$$

where ℓ is the arclength measured clockwise along the magnetic surface. Using Eq. (3) and changing the integration variable to x via $d\ell = \sqrt{1 + (dy/dx)^2}\, dx$,

$$q_{\text{MHD}} = \frac{B_\phi}{2\pi R_0} \frac{4Lq}{\kappa B_\phi} \int_{-x_0}^{x_0} \frac{dx}{\sqrt{(x_0^2 - x^2)\,(x_s^2 - x_0^2 + x^2)}} = q_c \frac{2}{\pi} \mathbf{K}(\rho), \tag{4}$$

where $q_c = L_q / R_0$ is the reference value of the safety factor obtained for circular flux surfaces, and

$$\mathbf{K}(\rho) \equiv \int_0^1 \frac{du}{\sqrt{(1-u^2)(1-\rho^2 u^2)}} = \int_0^1 \frac{dt}{\sqrt{(1-t^2)(1-\rho^2+\rho^2 t^2)}}$$

is the complete elliptic integral of first kind. The change of safety factor due to divertor geometry can be described by the expression, $q_{\text{MHD}}/q_c = \frac{2}{\pi}\mathbf{K}(\rho)$. We note the behavior of q_{MHD} in the $\rho \to 0$ (circular surface) and $\rho \to 1$ (separatrix) limits is described by:

$$\frac{q_{\text{MHD}}}{q_c} \sim \begin{cases} 1, & \rho \to 0 \quad \text{(circle)} \\ \frac{2}{\pi} \ln \frac{4}{\sqrt{1-\rho^2}}, & \rho \to 1 \quad \text{(separatrix)}. \end{cases}$$

The logarithmic divergence of q_{MHD} in the vicinity of separatrix is due to the fact that B_p vanishes at the x-points.

The global shear $\hat{s}$ can be defined by

$$\hat{s} = \frac{d \ln q_{\text{MHD}}}{d \ln \rho},$$

and expressed as

$$\hat{s} = \hat{s}_c + \frac{\mathbf{E}(\rho)}{\mathbf{K}(\rho)(1-\rho^2)} - 1, \tag{5}$$

where $\hat{s}_c = d\ln q_c / \ln \rho$ is the reference value of the global shear for a circular-flux-surface plasma, and $\mathbf{E}(\rho) \equiv \int_0^1 dt \sqrt{\frac{1-\rho^2 t^2}{1-t^2}}$ is the complete elliptic integral of second kind. The asymptotic behavior of $\hat{s} - \hat{s}_c$ is given by

$$\frac{\mathbf{E}(\rho)}{\mathbf{K}(\rho)(1-\rho^2)} - 1 \sim \begin{cases} \frac{1}{2}\rho^2, & \rho \to 0 \quad \text{(circle)} \\ \frac{1}{(1-\rho^2)\ln\left(1/\sqrt{1-\rho^2}\right)}, & \rho \to 1 \quad \text{(separatrix).} \end{cases}$$

Therefore, near the separatrix, the global shear diverges more rapidly (algebraically) than q_{MHD}, which diverges logarithmically. By way of illustration, q_{MHD}/q_c and $\hat{s}/\hat{s}_c$ are plotted as functions of ρ in Fig. 2.

III. Stability of Resistive Kink Modes in Diverted Tokamak Geometry

In general, the tearing mode stability parameter Δ' depends on the detailed radial profile of the current $J_0(r)$ and must be evaluated numerically. However for high-m tearing modes, even the kink-type "exterior" perturbations are sufficiently localized so that it is possible to evaluate Δ' using local parameters for the appropriate rational surface, in particular $\partial J_0(r)/\partial r$. In this section, we calculate Δ' for localized edge resistive kink modes in diverted tokamak geometry. In the case of H-mode discharges, temperature and current gradients are quite steep at the edge. Therefore, it is interesting to explore the competition between the strongly destabilizing current gradient and the stabilizing global shear. We also note that high q_{MHD} near the edge also extends the relevance of this analyses to low-n modes.

Ideal kink perturbations (exterior solution) in the vicinity of a rational surface r_0 are described by

$$\vec{B}_0 \cdot \nabla \frac{j_\parallel}{B} + \delta\vec{B} \cdot \nabla \frac{J_0}{B} = 0, \tag{6}$$

where in this section, the curvature term has been neglected for simplicity. The radial localization of the mode allows us to employ the ballooning mode formalism to write Eq. (6) as an ordinary differential equation in ℓ. We can therefore write any perturbed quantity $\tilde{A} \to \tilde{A}(\ell)e^{inS}$, where $\vec{B} \cdot \nabla S = 0$. Since the ballooning mode formalism allows

us to describe a resistive mode at a particular flux surface using equilibrium quantities specified for that flux surface, we can follow the procedure developed by Mercier and Luc[24] to calculate the various relevant quantities. This procedure is given in some detail in Ref. 21, and will not be repeated here.

In particular, the following results from Ref. 21 are useful to us: the eikonal S satisfies

$$\frac{\partial S}{\partial \ell} = -\frac{B_\phi}{R_0 B_p}, \tag{7a}$$

$$|\nabla S|^2 = \frac{B_\phi^2}{R_0^2}\left\{\frac{1}{B_p^2} + P(\ell)^2\right\}, \tag{7b}$$

where

$$P(\ell) = B_p \int_{\ell_0}^{\ell} \frac{d\ell}{B_p^3}\left\{\frac{\sigma B_{po}}{r_0} + \frac{2B_p}{R} - \frac{\alpha B_{po}}{r_0^2}\int_0^{\ell} \cos u d\ell\right\} \tag{7c}$$

characterizes the secularity of radial component of wave vector in ℓ,

$$\sigma = \frac{\partial}{\partial \psi}\left[P_0 + \frac{B_\phi^2}{2}\right]\frac{R_0 r_0}{B_{po}} \tag{7d}$$

is proportional to toroidal current density, and

$$\alpha = -\frac{2\partial P_0}{\partial \psi}\frac{r_0^2}{B_{po}} \tag{7e}$$

is the pressure gradient parameter.

Using the ideal MHD constraint $E_\parallel = 0$, and Ampere's law, Eq. (6) can be written in terms of the electrostatic potential ϕ,

$$B_p \frac{\partial}{\partial \ell}\left\{\frac{1}{B_p^2} + P(\ell)^2\right\} B_p \frac{\partial}{\partial \ell}\phi + \frac{i\mathcal{J}' B_p}{R_0 B_{po}}\frac{\partial}{\partial \ell}\phi = 0, \tag{8}$$

where $\mathcal{J}' \equiv B_{po} R_0^3 \partial J_0 / nB\partial\psi$ is a dimensionless parameter proportional to $\partial J_0/n\partial r$. Integrating Eq. (8) twice, and retaining the tearing parity (odd ϕ) piece, we have

$$\phi = \sin\left\{\frac{\mathcal{J}'}{R_0 B_{po}} I(\ell)\right\}, \tag{9}$$

where

$$I(\ell) = \int_0^{\ell} \frac{d\ell}{1/B_p + B_p P(\ell)^2}.$$

To facilitate further analytical progress, we make the approximations described below. First, since the modes are sharply localized in radius so that they extend several connection

lengths along $\vec{B}$ field lines, they naturally "sense" flux-surface-averaged quantities, i.e., global shear $\hat{s}$ and safety factor $q_{\rm MHD}$. Then, for large ℓ

$$P(\ell) \cong \frac{\hat{s}}{r_0}\frac{B_p}{B_{po}}\left\langle\frac{1}{B_p}\right\rangle\ell. \tag{10}$$

This approximation for $P(\ell)$ is used throughout this paper. Second, the smallness of B_p near the x-point does not affect the large-ℓ asymptotic behavior of $I(\ell)$ (which is all that is necessary for calculation of Δ'). This is because the influence of $1/B_p$ in the denominator of the integrand becomes progressively less important as ℓ increases. Then, we can make the approximations

$$\begin{aligned} I(\ell) &\cong \int_0^\ell \frac{d\ell}{1/B_{po} + \left(\hat{s}/r_0\right)^2 B_{po}\left\langle 1/B_p\right\rangle^2\ell^2} \\ &\cong \frac{r_0}{\hat{s}}\left\langle 1/B_p\right\rangle^{-1}\tan^{-1}\left(\frac{\hat{s}}{r_0}B_{po}\left\langle 1/B_p\right\rangle\ell\right). \end{aligned} \tag{11}$$

The large ℓ behavior of ϕ is then given by

$$\begin{aligned} \phi &\cong \sin\left[\frac{r_0\mathcal{J}'}{R_0\hat{s}B_{po}}\left\langle 1/B_p\right\rangle^{-1}\left(\frac{\pi}{2} - \frac{r_0\left\langle 1/B_p\right\rangle^{-1}}{\hat{s}B_{po}\ell}\right)\right] \\ &\cong \sin\left(\frac{\pi}{2}\Sigma\right) - \frac{r_0\left\langle 1/B_p\right\rangle^{-1}}{\hat{s}B_{po}}\Sigma\cos\left(\frac{\pi}{2}\Sigma\right)\frac{1}{\ell}, \end{aligned} \tag{12a}$$

where

$$\Sigma \equiv \frac{r_0}{R_0}\frac{\mathcal{J}'}{\hat{s}B_{po}}\left\langle 1/B_p\right\rangle^{-1}. \tag{12b}$$

Finally, from Eq. (12b)

$$\Delta' = -\frac{\pi n q_{\rm MHD}^2\hat{s}}{r_0^2 q_c}\left\{\frac{\frac{r_0\left\langle 1/B_p\right\rangle^{-1}}{\hat{s}B_{po}}\Sigma\cos\left(\frac{\pi}{2}\Sigma\right)}{\sin\left(\frac{\pi}{2}\Sigma\right)}\right\} = -\frac{2nq_{\rm MHD}}{r_0}\frac{\pi}{2}\Sigma\cot\left(\frac{\pi}{2}\Sigma\right). \tag{13}$$

It follows that when m becomes large, for fixed $\frac{\partial J_0}{\partial r}$, $\Sigma \to 0$ so that we recover well known result $\Delta' = -2nq_{\rm MHD}/r_0$. $\frac{r_0\Delta'}{nq_{\rm MHD}}$ is plotted as a function of Σ in Fig. 3. We note that Δ' becomes positive at $\Sigma = 1$ corresponding to the destabilization of resistive kink modes. We also note that Δ' abruptly changes from $+\infty$ to $-\infty$ (i.e., marginal ideal kink stability) at $\Sigma = 2$. Expressing Σ (Eq. (12b)) in terms of physical variables assuming

$$\left.\frac{d\ln B_p}{d\ln r}\right|_{r_0} < 1,$$

we note resistive kink stability follows for

$$\frac{r_0}{L_J} < n q_{\text{MHD}} \hat{s}, \tag{14}$$

where

$$L_J^{-1} = -\frac{d \ln J_0(r)}{dr}.$$

This formula suggests that resistive kink modes are stable in the presence of large current density gradients when the resonant surface lies in the high global shear and q_{MHD} regions. As shown in Sec. II, q_{MHD} and $\hat{s}$ become quite large near the separatrix. Thus, improved stability against resistive kink modes follows. Finally, it should be noted that improved resistive kink stability only results when the steep current gradient falls in the region of large $q_{\text{MHD}}\hat{s}$. Hence, it appears that H-mode plasmas, with relatively broad profiles, exploit the enhanced global shear of separatrix geometry more efficiently than their L-mode counterparts do.

IV. Linear Theory of Resistive Ballooning Modes in Divertor Geometry

The procedure for deriving the resistive ballooning mode dispersion relation appropriate to a large aspect ratio, nearly circular-flux-surface plasma (for example, the $\hat{s}-\alpha$ model[25]) is well known.[26,27] In this section, we study the linear theory of the resistive ballooning instability in divertor geometry. In particular, the assumption of near circular flux surfaces is relaxed.

For convenience, we choose the simplest possible physical model containing the necessary constituents of resistive ballooning modes, i.e., the reduced resistive MHD model[28] where pressure evolves by fluid convection. The effects of plasma compression[26,28–30] and diamagnetic drift[27] are ignored. The following set of equations constitutes the theoretical model for linear resistive ballooning instability.

i) Ohm's law:

$$\eta j_\parallel = -\hat{b} \cdot \nabla \phi + \Gamma A_\parallel, \tag{15}$$

where $\eta = m_e \nu_{ei}/n_0 e^2$ is the Spitzer resistivity, Γ the linear growth rate and the other notation is standard.

ii) Vorticity equation:

$$\frac{\rho_m \Gamma}{B^2}\nabla_\perp^2 \phi - \vec{B}\cdot\nabla\frac{j_\parallel}{B} + \frac{2\vec{\kappa}\times\vec{B}}{B^2}\cdot\nabla\tilde{p} = 0, \tag{16}$$

where $\vec{\kappa} = \hat{b}\cdot\nabla\hat{b}$ is the curvature, ρ_m the mass density, and $\tilde{p}$ the perturbed pressure.

iii) Pressure convection equation:

$$\Gamma\tilde{p} + \vec{v}_E\cdot\nabla P_0 = 0, \tag{17}$$

where $\vec{v}_E = -\nabla\phi\times\hat{b}/B$ is the $\vec{E}\times\vec{B}$ fluid velocity.

In ballooning coordinates, the curvature (ballooning drive) term can be written as

$$\frac{\vec{B}\times\nabla S\cdot\vec{\kappa}}{B^2} = \frac{1}{R_0^2}\left\{\frac{\sin u}{B_p} + P(\ell)\cos u\right\}, \tag{18}$$

where the first and second term on the RHS represent the normal and geodesic components, respectively.

Using Eqs. (17) and (7a), the perturbed pressure can be written as

$$\tilde{p} = \frac{in}{\Gamma}\frac{\partial P_0}{\partial\psi}\phi, \tag{19}$$

and can be eliminated from Eqs. (16) and (17) yielding

$$\eta j_\parallel + \frac{B_p\partial}{B_\phi\partial\ell}\phi - \Gamma A_\parallel = 0, \tag{20}$$

$$B_p\frac{\partial}{\partial\ell}j_\parallel + \frac{n^2}{\Gamma}\frac{\alpha B_{po}B_\phi}{r_0^2R_0^2}\left(\frac{\sin u}{B_p} + P(\ell)\cos u\right)\phi + \rho_m n^2\Gamma\frac{B_\phi}{R_0^2}\left\{\frac{1}{B_p^2} + P(\ell)^2\right\}\phi = 0. \tag{21}$$

The curvature (the second term in Eq. (21)) varies along the magnetic field line with characteristic scale length qR (connection length), while the eigenmode tends to extend along the equilibrium magnetic field line in order to minimize the stabilizing influence of field line bending. Thus, two disparate length scales are present in the problem, and we thus apply the two-scale expansion procedure. In this procedure, the flux surface average over the (short) connection length scale yields the eigenmode equation with (long) resistive length scale $\sim \eta^{-1/3}$. This calculation is straightforward but tedious, and is complicated by

divertor geometry. Thus, we continue our analysis by considering the flux-surface-averaged eigenmode equation.

$$\frac{\partial}{\partial \ell}\frac{\left(\frac{B_\phi}{R_0}\frac{\hat{s}}{r_0 B_{po}}\right)^2 \ell^2}{\left\langle 1/B_p^3\right\rangle \Big/ \left\langle 1/B_p\right\rangle^3 + \frac{\eta n^2}{\Gamma}\left(\frac{B_\phi \hat{s}}{R_0 r_0 B_{po}}\right)^2 \ell^2}\frac{\partial}{\partial \ell}\Phi^{(0)} = \frac{B_\phi^2}{R_0^2}\left\langle \frac{1}{B_p}\right\rangle \left(\rho_m \Gamma^2 \left\langle B_p\right\rangle - \left(\frac{\alpha B_{po}}{r_0^2}\right)^2 \frac{\eta n^2 B_\phi}{\Gamma R_0^2}\left\langle \frac{x^2}{B_p}\right\rangle\right) \times \left(\frac{\hat{s}}{r_0 B_{po}}\right)^2 \left\langle \frac{1}{B_p}\right\rangle^2 \ell^2 \Phi^{(0)}, \tag{22}$$

where $\langle A\rangle = \oint d\ell A / \oint d\ell$. In the derivation, a small contribution from the average curvature (magnetic well) has been ignored. The LHS (left-hand side) of Eq. (22) represents the effect of resistivity modified field line bending, while the first and second term of the RHS (right-hand side) represent inertia and the instability driving force, respectively. We note that the destabilizing driving force originates from the *beating* of the oscillatory perturbed pressure and geodesic curvature, both of which vary along ℓ with scale r_0. This underscores the essential difference between the resistive ballooning mode and the resistive interchange mode, which is driven by bad *average* curvature and the pressure gradient.

The stabilizing effect of field line bending is weakened by resistive dissipation at large ℓ, and when $\ell^2 > \left(\Gamma/\eta n^2\right)^{-1}\left(B_\phi \hat{s}/R_0 r_0 B_{po}\right)^2 \left\langle 1/B_p^3\right\rangle / \left\langle 1/B_p\right\rangle^3$, the simplifying electrostatic approximation is possible. In this limit, Eq. (13) becomes

$$\frac{\partial^2}{\partial \ell^2}\Phi^{(0)} = \frac{\eta n^2 B_\phi^2}{\Gamma R_0^2}\left\langle \frac{1}{B_p}\right\rangle \left\{\rho_m \Gamma^2 \left\langle B_p\right\rangle - \left(\frac{\alpha B_{po}}{r_0^2}\right)^2 \frac{\eta n^2 B_\phi^2}{\Gamma R_0^2}\left\langle \frac{x^2}{B_p}\right\rangle\right\} \times \left(\frac{\hat{s}}{r_0 B_{po}}\left\langle \frac{1}{B_p}\right\rangle\right)^2 \ell^2 \Phi^{(0)}. \tag{23}$$

As Eq. (14) is a Weber equation, the growth rate for most unstable mode is given by

$$\Gamma^3 = \frac{\eta n^2 B_\phi^2}{\rho_m R_0^2}\left(\frac{\alpha B_{po}}{r_0^2}\right)^2 \frac{\left\langle x^2/B_p\right\rangle}{\left\langle B_p\right\rangle}. \tag{24}$$

The existence of an effective potential well for Eq. (14) can be shown by retaining small corrections to Eq. (23) such as the k_θ^2 correction to $\nabla_\perp^2$.[27] Note that Eq. (24) can be written in a more illuminating way,

$$\Gamma = f_\Gamma(\rho)\Gamma^0, \tag{25a}$$

where

$$\Gamma^0 = \left(\frac{n^2}{S_m}\right)^{1/3} \alpha^{2/3} \tau_A^{-1}, \tag{25b}$$

$$S_m = \tau_R / \tau_A,$$

$$\tau_R = a^2/\eta,$$

$$\tau_A^{-1} = \frac{B_\phi}{R_0 \sqrt{\rho_m}}.$$

Γ^0 is the usual result[15] obtained for a circular-flux-surface plasma, and $f_\Gamma(\rho)$ is a multiplicative factor characterizing the effect of divertor geometry. After some straightforward algebra, we find that

$$f_\Gamma(\rho) = 3^{2/3} \left[\frac{\mathbf{E} - (1-\rho^2)\mathbf{K}}{(1+\rho^2)\mathbf{E} - (1-\rho^2)\mathbf{K}}\right]^{2/3}, \tag{26a}$$

with

$$f_\Gamma(0) = 1 \tag{26b}$$

$$f_\Gamma(1) = (1.5)^{2/3} \approx 1.31. \tag{26c}$$

Note that there is no explicit dependence of Γ on either $\hat{s}$ or q_{MHD}, and thus the growth rate is basically unaffected by the divertor geometry.

We also evaluate the eigenmode width, for future use. The eigenmode width, determined by the asymptotic balance of the line-bending and inertia terms, is given by

$$\ell_w^{-4} = r_0^{-4} \left[\frac{n^2}{S_m} \frac{\hat{s}^2}{\rho^2} \Gamma \tau_A q_{\text{MHD}}^3 q_c\right], \tag{27}$$

where $\langle B_p \rangle \cong B_{po}$ has been used.

V. Saturated Resistive Fluid Turbulence and the Associated Anomalous Electron Thermal Conductivity

Having obtained expressions for the global shear, safety factor, linear growth rate, and mode width of the resistive ballooning mode in divertor geometry, we now discuss the nonlinear saturation mechanism and calculate the resulting anomalous electron thermal conductivity due to magnetic fluctuations generated by resistive ballooning modes in a diverted tokamak plasma. Previous work[15] on the nonlinear evolution of resistive ballooning modes has shown that the dominant nonlinear effect is due to the pressure-convection

nonlinearity, which modifies the turbulent response of pressure $\tilde{p}$ to potential fluctuations ϕ. This causes a reduction of the destabilizing term while preserving the basic structure of the eigenmode. Therefore, in the nonlinear phase, the eigenmode structure is properly described within the electrostatic approximation, and the radial mode width Δ remains as the effective nonlinear "mixing length." That is, resistive ballooning modes saturate when the pressure fluctuation mixes dP/dr over the radial extent Δ of each poloidal subharmonic. Thus, the pressure fluctuation at saturation is given approximately by the "mixing length" relation

$$\tilde{P}/P_0 \simeq \Delta/L_p, \quad \text{where} \quad L_p^{-1} = -\frac{d\ln P_0}{dr}.$$

Therefore, the saturated turbulent potential fluctuation driven by these modes is given by

$$\left(\frac{nq_c}{B_\phi r_0}\right)^2 |\phi|^2 = \Gamma^2\Delta^2. \tag{28}$$

Here, Eq. (10) has been used to relate ϕ and $\tilde{p}$.

Using a standard iterative renormalization method, we can show that at saturation, the turbulent convection process can be represented by turbulent radial diffusion with coefficient $D \approx \Gamma\Delta^2$. In physical terms, the turbulent convection results in a decorrelation time τ_{cn} $(\simeq \Delta^2/D)$ such that $\tau_{cn}^{-1} = \Gamma$, i.e., a pressure element responding to the driving forces is decorrelated at a rate equal to the rate of growth caused by the driving forces. The expression for Δ can be obtained using the reciprocal relation between the ballooning coordinate ℓ, and radial distance from a rational surface, i.e.,

$$\Delta/r_0 = \left(nq_{\rm MHD}B_p\hat{s}\ell_w/B_{po}r_0\right)^{-1}, \tag{29}$$

where ℓ_w is the mode width along the equilibrium magnetic field line given by Eq. (27). Note that Eqs. (27) and (29) imply that $\Delta \sim \hat{s}^{-1/2}$, i.e., the large shear near the separatrix makes the radial mixing length smaller. Using Eq. (29), we can obtain the resulting convective diffusion coefficient $D \sim \hat{s}^{-2}\left(P_0q^2/\epsilon L_pB_\phi^2\right)a^2/\tau_R$, which is small compared to most experimentally determined values of the thermal diffusivity.

Another, more significant consequence of saturated resistive ballooning mode turbulence is anomalous electron heat conduction induced by the magnetic field line stochastization. Although the basic mode structure and dynamics are successfully described within

the electrostatic theory, the resistive ballooning mode also produces a radial magnetic field perturbation which can be obtained using Ohm's law, i.e.,

$$-\eta j_{\|} = \eta \nabla_{\perp}^2 A_{\|} \cong \frac{B_p}{B_\phi} \frac{\partial}{\partial \ell} \phi. \tag{30}$$

Now, we can estimate the anomalous electron thermal conductivity $\chi_e \simeq \frac{3}{2} v_{te} D_M$ by calculating the stochastic magnetic field line diffusion coefficient D_M, following the procedure of Ref. 15. We note that D_M was calculated for the relevant strong turbulence regime, where $D_M \propto |\delta B/B_0|$. From Ref. 15, D_M is given by

$$D_M \simeq \left[\frac{\sum_{n'} \sum_{m'} \left| A_{\|n'}(y + 2\pi m') \right|^2}{B_\phi^2 \hat{s}^2 (\ell_w / r_0)^2} \right]^{1/2}. \tag{31}$$

Substituting Eq. (30) into Eq. (31) and using Eq. (28) yields

$$D_M \simeq \frac{q_{\text{MHD}}/q_c}{\eta R q_c} \sum_n \left(\frac{n q_{\text{MHD}} \hat{s} \ell_w}{r_0} \right)^{-4} \frac{\Gamma r_0^5}{\ell_w}. \tag{32}$$

Finally, by extracting the $\hat{s}$ and q_{MHD} dependence of D_M using Eq. (27), we can write the anomalous electron thermal conductivity $\chi_e = \frac{3}{2} v_{Te} D_M$ as

$$\chi_e = f_\chi(\rho) \chi^0, \tag{33a}$$

where

$$\chi^0 = \frac{3}{2} v_{te} a \frac{q_c}{S_m} \left(\frac{\alpha}{\hat{s}_c} \right)^{3/2}, \tag{33b}$$

$$f_\chi(\rho) = \left(\frac{\hat{s}}{\hat{s}_c} \right)^{-3/2} \left(\frac{q_{\text{MHD}}}{q_c} \right)^{3/4} f_\Gamma(\rho)^{9/4}. \tag{33c}$$

χ^0 is the result of Ref. 15 which was obtained for near circular-flux-surface plasmas. The effects of divertor geometry are represented by the multiplicative factor $f_\chi(\rho)$ which has the following asymptotic behavior

$$f_\chi(\rho) \to \begin{cases} 1, & \rho \to 0 \\ \hat{s}_c^{3/2} \left(3^2/2\pi\right)^{3/4} (1-\rho^2)^{3/2} \left(\ln \frac{1}{\sqrt{1-\rho^2}} \right)^{9/4}, & \rho \to 1. \end{cases}$$

Note that Eq. (33) offers the possibility of improvement energy confinement by strong shear even with steep pressure gradients. $f_\chi(\rho)$ is plotted in Fig. 4 as a function of ρ for $\hat{s}_c = 1$ and $\hat{s}_c = 2$. Note the considerable reduction of χ_e relative to χ^0 when $\rho \gtrsim .8$ (or roughly $r \gtrsim .8a$). This reduction of thermal conductivity is due primarily to enhanced shear near the separatrix, since, as noted earlier, the increase in the safety factor q_{MHD} due to divertor geometry is less singular than the increase in the global shear. We also note that the effective radial mixing length scales favorably with shear $\Delta \approx r_0 \left(n q_{\text{MHD}} \hat{s} \ell_w\right)^{-1} \sim \hat{s}^{-1/2}$, and thus the saturated root mean-squared electrostatic potential and electromagnetic potential fluctuations also scale favorably with shear, i.e., $\left\langle \phi^2 \right\rangle^{1/2} \sim \Delta\Gamma \sim \hat{s}^{-1/2}$, and $\left\langle A_\parallel^2 \right\rangle^{1/2} \sim \frac{\Delta^2}{\ell_w} \left\langle \phi^2 \right\rangle^{1/2} \sim \hat{s}^{-1}$. Finally, it is interesting to note that the increased global shear has considerably more impact on the thermal diffusivity and fluctuation levels than on the linear growth rate of the resistive ballooning mode.

VI. Particle Transport in Diverted Tokamak Edge Plasmas

As shown in Sec. V, convective particle loss induced by resistive pressure gradient driven turbulence is small in comparison to thermal conduction loss. However, edge particle transport in tokamaks is consistently observed to be anomalous, with particle diffusivity $D_n \sim 10^4 - 10^5 cm^2/\text{sec}$. Indeed, in some tokamak edge plasmas, particle convection has been found to be the dominant loss mechanism.[14,31,32] The recently advanced theory of impurity gradient driven turbulence[20] (IGDT) is a resistive fluid turbulence model with several promising features of relevance to tokamak edge fluctuation phenomena. In this section we consider IGDT both as a general resistive fluid paradigm for, and detailed model of, particle transport in divertor tokamaks. Since the details of IGDT theory are presented in Ref. 20, we simply describe the theoretical model and state the results and their consequences in this section.

The theoretical model for IGDT consists of the electrostatic reduced resistive MHD equations

$$-\nabla_\parallel \phi = \tilde{\eta} J_{\parallel 0} + \eta_0 \tilde{J}_\parallel, \tag{34}$$

$$\rho_m \frac{d}{dt} \nabla_\perp^2 \phi = B_\phi \nabla_\parallel \tilde{J}_\parallel, \tag{35}$$

where resistivity dynamics is described by temperature and $Z_{\rm eff}$ evolution equations

$$\frac{d}{dt}\tilde{\eta}_{\rm sp} - \nabla_{\|}\chi_T\nabla_{\|}\tilde{\eta}_{\rm sp} = -\frac{ik_\theta}{B_\phi}\phi\frac{\partial\eta_{\rm sp,0}}{\partial r}, \tag{36}$$

$$\frac{d}{dt}\tilde{Z}_{\rm eff} - \nabla_{\|}\chi_Z\nabla_{\|}\tilde{Z}_{\rm eff} = -\frac{ik_\theta}{B_\phi}\phi\frac{\partial Z_{\rm eff,0}}{\partial r}, \tag{37}$$

where $\eta = \eta_{\rm sp}(T_e)Z_{\rm eff}$, $\eta_{\rm sp} = m_e\nu_{ei}(T_e)/n_0e^2$ is the Spitzer resistivity, $Z_{\rm eff} = 1 + Z^2n_I/n_i$ for the prototypical case of a single, low-Z impurity species with charge Z and density n_I, χ_T is the parallel thermal conductivity, and $\chi_Z = v_{{\rm th},i}^2/Z^2\nu_{ii}$ is an effective transport coefficient for impurity flow along field lines. In Eq. (37), which was originally derived in Ref. 33, the parallel diffusion operator $\nabla_{\|}\chi_Z\nabla_{\|}$ follows from the fact that parallel impurity flow is determined by the balance of the parallel impurity pressure gradient with impurity-ion friction.

In the course of nonlinear evolution the current perturbation $\tilde{J}_{\|}$, which is peaked near $\vec{k}\cdot\vec{B}_0 = 0$ resonant surface, decouples from $\tilde{\eta}_{\rm sp}$, $\tilde{Z}_{\rm eff}$, and ϕ. Therefore, the vorticity equation becomes irrelevant, and the Ohm's law can be simplified to

$$-\nabla_{\|}\phi = \tilde{Z}_{\rm eff}\eta_{\rm sp,0}J_{\|0} + Z_{\rm eff,0}\tilde{\eta}_{\rm sp}J_{\|0}. \tag{38}$$

The convective nonlinearity in Eqs. (36) and (37) can be renormalized using standard iterative methods[19] yielding

$$\left(\frac{\partial}{\partial t} - \chi_T\nabla_{\|}^2\right)\tilde{\eta}_{\rm sp} - D^T\frac{\partial^2}{\partial x^2}\tilde{\eta}_{\rm sp} = -\frac{ik_\theta\phi}{B_\phi}\frac{\partial\eta_{\rm sp,0}}{\partial r}, \tag{39}$$

$$\left(\frac{\partial}{\partial t} - \chi_Z\nabla_{\|}^2\right)\tilde{Z}_{\rm eff} - D^Z\frac{\partial^2}{\partial x^2}\tilde{Z}_{\rm eff} = -\frac{ik_\theta\phi}{B_\phi}\frac{\partial Z_{\rm eff,0}}{\partial r}, \tag{40}$$

where

$$D^T = \sum_{\vec{k}'} k_\theta'^2\left|\phi_{\vec{k}'}\right|^2\left[\gamma_{\vec{k}+\vec{k}'} + \chi_T\left(\vec{k}_{\|} + \vec{k}_{\|}'\right)^2\right]^{-1}$$

and

$$D^Z = \sum_{\vec{k}'} k_\theta'^2\left|\phi_{\vec{k}'}\right|^2\left[\gamma_{\vec{k}+\vec{k}'} + \chi_Z\left(\vec{k}_{\|} + \vec{k}_{\|}'\right)^2\right]^{-1}$$

describe the crucial nonlinear effect of random convection of resistivity and impurity density by fluid turbulence. At saturation, Eqs. (39) and (40) can be solved approximately to

determine the saturated turbulence levels using Eq. (38) to eliminate ϕ. The characteristic radial scales for $\tilde{\eta}_{\rm sp}$ and $\tilde{Z}_{\rm eff}$, which are determined from asymptotic balance of $\chi_T \nabla_\parallel^2$ or $\chi_Z \nabla_\parallel^2$ with turbulent diffusion of $\tilde{\eta}_{\rm sp}$ or $\tilde{Z}_{\rm eff}$, are respectively,

$$\Delta^T = \left[\frac{D^T L_s^2}{\chi_T k_\theta^2}\right]^{1/4}$$

and

$$\Delta^Z = \left[\frac{D^Z L_s^2}{\chi_Z k_\theta^2}\right]^{1/4}.$$

The thermal and impurity diffusivities are

$$D^T = \left[\frac{E_0 L_s}{B_\phi L_\eta}\left(1+\eta_Z\right)\right]^{4/3} \Big/ \left(\chi_T \bar{k}_\theta^2 / L_s^2\right)^{1/3}, \tag{41}$$

and

$$D^Z = \left[\frac{E_0 L_s}{B_\phi L_\eta}\left(1+\eta_Z\right)\right]^{4/3} \Big/ \left(\chi_Z \bar{k}_\theta^2 / L_s^2\right)^{1/3}, \tag{42}$$

where $\eta_Z = L_\eta / L_Z$, $L_\eta^{-1} = d\ln\eta_{\rm sp}/dr$, $L_Z^{-1} = d\ln Z_{\rm eff}/dr$, $E_0 = \eta_{{\rm sp},0} Z_{{\rm eff},0} J_{\parallel 0}$, and $\bar{k}_\theta$ indicates a spectrum-averaged value. The mean-square turbulent radial velocity is given by

$$\left\langle \hat{v}_r^2 \right\rangle = \left[\frac{E_0 L_s}{B_\phi L_\eta}\left(1+\eta_Z\right)\right]^2. \tag{43}$$

A key difference between impurity and temperature dynamics is that in contrast to $\eta_{\rm sp}(r)$, which virtually always increases with radius, the $Z_{\rm eff}(r)$ profile may peak either on axis ($\eta_Z < 0$) or at edge ($\eta_Z > 0$). Thus, the impurity gradient can either enhance (edge-peaked $Z_{\rm eff}(r)$) or oppose (axially-peaked $Z_{\rm eff}(r)$) the temperature gradient drive, i.e., note the $\left(1+\eta_Z\right)^2$ dependence in Eq. (43).

Since the characteristic spatial scale for working gas ion density fluctuations is also given by Δ^Z, it follows that the cross-field particle diffusivity is

$$\begin{aligned} D_n &\cong \left[\frac{E_0 L_s}{B_\phi L_\eta}\left(1+\eta_Z\right)\right]^{4/3} \left(\chi_Z \bar{k}_\theta^2 / L_s^2\right)^{-1/3} \\ &\sim T^{-5/6} \frac{q^2 R^2}{\hat{s}^2} n^{1/3} B_\phi^{-4/3} V_L^{4/3} \left(L_\eta^{-1} + L_Z^{-1}\right)^{4/3}. \end{aligned} \tag{44}$$

Note that Eq. (44) offers the possibility of reconciling high edge temperature and strong shear with improved particle confinement and steep temperature gradients.

Equation (44) can be extended to divertor geometry by replacing $\hat{s}$ and q_{MHD} with expressions which include effects specific to divertor geometry. This "substitution rule" can be easily verified by performing a flux surface average of Eqs. (34)–(37). In the absence of toroidal coupling, i.e., ballooning terms, the derivation is straightforward. Equation (44) can thus be written as a product of a reference value D^0, for a circular-flux-surface plasma and various divertor geometry specific factors, i.e.,

$$D_n = \left(q_{\text{MHD}}/q_c\right)^2 \left(\hat{s}_c/\hat{s}\right)^2 D^0. \tag{45}$$

The ratio D_n/D^0 is plotted as a function of the flux surface shape parameter ρ in Fig. 5. Note the appreciable reduction of particle loss due to increased global shear when $\rho \gtrsim .9$ and the initial departure from the circular-flux-surface model at $\rho \simeq .8$. For ASDEX, $a = 40$ cm so that these radii correspond to $r = 36$ cm and $r = 32$ cm, respectively.

VII. Speculations on the $L \rightarrow H$ Transition

In this paper, resistive fluid turbulence in diverted tokamak edge plasmas has been examined. The principal results of this paper are:

i) the thermal and particle diffusivities corresponding to resistive pressure gradient driven and resistivity gradient driven turbulence are calculated for separatrix geometry.

ii) the principal effect of separatrix geometry on resistive fluid turbulence is a decrease in the characteristic radial scale length (step size) due to increased global shear.

iii) resistive kink stability of modes resonant near the separatrix is also shown to follow from the increased values of global shear and safety factor characteristic of that region.

iv) the reduced radial scale length results in reduced χ_E and D_n near the separatrix ($\rho > .9$), consistent with the notion of a transport barrier. In addition, reduced Δr results in reduced magnetic fluctuation levels, consistent with good runaway confinement in H-mode.

v) for ASDEX, the zone of improved confinement is predicted to be localized to $r > 36$cm, with departure of $\chi_E(r)$ from its circular-flux-surface analogue beginning at $r = 32$ cm. These predictions are in reasonable agreement with the results of transport analyses.[7]

vi) two scenarios related to the $L \rightarrow H$ transition are proposed. These are based on the dynamics of resistive fluid turbulence, and depend on the interplay of various physical processes discussed in this paper.

While this paper has discussed the effects of divertor geometry on tokamak edge plasma stability and turbulence, the subject of how the potentially good confinement zone is actually utilized in H-mode, i.e., the nature of the $L \rightarrow H$ transition, has not yet been addressed. Here, two scenarios are proposed and related issues are discussed.

First, one rather straightforward scenario is that improved particle confinement (reduced D_n), and the accompanying steepening of L_n^{-1} near the edge, lead to diamagnetic stabilization of ideal ballooning modes, thus allowing the plasma to support large pressure gradients. Improved particle confinement follows from the result of Section VI $D_n \sim T^{-5/6} \left(q^2/\hat{s}^2\right) L_T^{-4/3}$, i.e., steep gradients can be supported in the region of strong global shear near the separatrix, and confinement improves when the edge temperature increases. Consequently, the density gradient steepens and the diamagnetic frequency $\omega_* \sim T/L_n$ also increases. Noting that ideal ballooning modes satisfy the familiar dispersion relation

$$\omega = -\frac{\omega_{*i}}{2} \pm \frac{1}{2}\left(\omega_{*i}^2 - 4\gamma_{\text{MHD}}^2\right)^{1/2},$$

where $\gamma_{\text{MHD}}^2 \sim \left(c_s^2/L_p R\right)\left(1 - L_p\beta_c/L_{p\,\text{crit}}\beta\right)$ is the ideal ballooning mode growth rate, it follows that ballooning stability is guaranteed for modes with

$$k_\theta^2 \rho_i^2 > \frac{2L_n}{L_p}\frac{L_n}{R}\left(1 - \frac{L_p\beta_c}{L_{p\,\text{crit}}\beta}\right).$$

For ASDEX parameters ($L_n \sim L_p \sim 3$ cm, $R \sim 165$ cm), this corresponds to $k_\theta \rho_i > .1$, a range which encompasses the large-n modes which can be treated using ballooning mode formalism. Thus, it appears that improved edge particle confinement accompanied by increased edge temperature enables the plasma to support the large edge pressure gradients

characteristic of H-mode. It should be noted that this scenario is consistent with the observations that reduced H_α emission and increased ion edge temperatures accompany the onset of H-mode. Also, this scenario is less sensitive to the details of x-point configuration, etc., than those based exclusively on ideal MHD stability. Finally, it should also be noted that steepening of the density gradient also ensures stability to ion temperature gradient driven modes.

Second, it is interesting to note that the resistive pressure gradient-driven turbulence model thermal diffusivity $\chi_e \sim (1/T_e)(\alpha/\hat{s})^{3/2}$ offers the possibility of reconciling good energy (and runaway) confinement (χ_e small) and steep pressure gradient (α large) with high edge temperature and strong global shear (T_e, $\hat{s}$ large). In particular, large edge temperature gradients can be supported in the region of enhanced global shear ($\rho \gtrsim .9$). Thus, one might propose a scenario whereby the edge χ_e drops as the edge T increases and the pressure profile broadens (as observed in H-mode) so that the gradient occupies the strong shear region. Also, the increased edge temperature and steepened density gradient result in enhanced compression[26,28–30] or diamagnetic[27] stabilization of the resistive ballooning mode, thus reinforcing the reduction in χ_e. Note that this scenario is both an alternative and a complement to the first one. Finally, detailed studies of the nature of the $L \rightarrow H$ bifurcations possible within these models require transport analyses, and will be discussed in future publications.

Both of the proposed scenarios are based on notions of enhanced stability to pressure gradient-driven modes. However, any H-mode scenario must also address the stability of current-gradient-driven modes. As demonstrated here, the enhanced global shear near the separatrix results in the stability of resistive kink modes resonant in that region. This observation, along with those pertaining to improved edge confinement, is consistent with the broad current profiles characteristic of H-mode plasmas. By maintaining the current gradient near the edge, such profiles have $q(0) > 1$ and are more stable to low-m tearing (dJ_0/dr at $q = 2$ is small!). Hence, sawteeth and significant MHD activity are absent. Thus, it appears that separatrix geometry enables H-mode plasma to assume more favorable current profiles. Indeed, it is intriguing to speculate that the enhanced global shear stabilizes the current-gradient-driven "consistency of plasma profile instability" invoked

by phenomenological theories of profile consistency, so that H-mode plasmas do not suffer from L-mode losses.

Acknowledgements

The authors wish to acknowledge stimulating conversations with C. M. Bishop, J. W. Connor, R. J. Hastie, M. N. Rosenbluth, and F. Wagner. This research was supported by U. S. Department of Energy Contract #DE-FG05-80ET-53088.

References

1. F. Wagner, G. Becker, K. Behringer, D. Campbell, A. Eberhagen, W. Engelhardt, G. Fussmann, O. Gehre, J. Gernhardt, G. v. Gierke, G. Haas, M. Huang, F. Karger, M. Keilhacker, O. Klüber, M. Kornherr, K. Lackner, G. Lisitano, G. G. Lister, H. M. Mayer, D. Meisel, E. R. Müller, H. Murmann, H. Niedermeyer, W. Poschenrieder, H. Rapp, H. Röhr, F. Schneider, G. Siller, E. Speth, A. Stäbler, K. H. Steuer, G. Venus, O. Vollmer, and Z. Yü, Phys. Rev. Lett. **49**, 1408 (1982).
2. S. M. Kaye, M. G. Bell, K. Bol, D. Boyd, K. Brau, D. Buchenauer, R. Budny, A. Cavallo, P. Couture, T. Crowley, D. S. Darrow, H. Eubank, R. J. Fonck, R. Goldston, B. Grek, K. P. Jaehnig, D. Johnson, R. Kaita, H. Kugel, B. Leblanc, J. Manickam, D. Manos, D. Mansfield, E. Mazzucato, R. McCann, K. McGuire, D. Mueller, A. Murdock, M. Okabayashi, K. Okano, D. K. Owens, D. E. Post, M. Reusch, G. L. Schmidt, S. Sesnic, R. Slusher, S. Suckewer, C. Surko, H. Takahashi, F. Tenney, H. Towner, and J. Valley, J. Nucl. Mater. **121**, 115 (1984).
3. K. H. Burrell and the Doublet-III Physics, Operations, and Neutral Beam Groups, in *Controlled Fusion and Plasma Physics*, (ECA, Linnich, 1983), Part I, p. 11.
4. M. Nagami, M. Kasai, A. Kitsunezaki, T. Kobayashi, S. Konoshima, T. Matsuda, N. Miya, H. Ninomiya, S. Sengoku, M. Shimada, H. Yokomizo, T. Angel, C. Armentrout, F. Blau, G. Bramson, N. Brooks, R. Chase, A. Colleraine, E. Fairbanks, J. Fasolo, R. Fisher, R. Groebner, T. Hino, R. Hong, G. Jahns, J. Kamperschroer, J. Kim, A. Lieber, J. Lohr, D. McColl, L. Rottler, R. Seraydarian, R. Silagi, J. Smith, R. Snider, T. Taylor, J. Tooker, D. Vaslow, S. Wojtowicz, Nucl. Fusion **24**, 183 (1984).
5. F. Wagner, G. Fussmann, T. Grave, M. Keilhacker, M. Kornherr, K. Lackner, K. McCormick, E. R. Müller, A. Stäbler, G. Becker, K. Bernhardi, U. Ditte, A. Eberhagen, O. Gehre, J. Gernhardt, G. v. Gierke, E. Glock, O. Gruber, G. Haas, M. Hesse, G. Janeschitz, F. Karger, S. Kissel, O. Klüber, G. Lisitano, H. M. Mayer, D. Meisel, V. Mertens, H. Murmann, W. Poschenrieder, H. Rapp, H. Röhr, F. Ryter, F. Schneider, G. Siller, P. Smeulders, F. Söldner, E. Speth, K. H. Steuer, Z. Szymanski, and O. Vollmer, Phys. Rev. Lett. **53**, 1453 (1984).
6. F. Wagner, and the ASDEX and NI teams, Private Communication.

7. O. Gruber, W. Jilge, K. Bernhardi, A. Eberhagen, G. Fussmann, O. Gehre, J. Gernhardt, G. v. Gierke, E. Glock, G. Haas, G. Janeschitz, F. Karger, M. Keilhacker, O. Klüber, M. Kornherr, K. Lackner, G. Lisitano, H. M. Mayer, K. McCormick, D. Meisel, V. Mertens, E. R. Müller, H. Niedermeyer, W. Poschenrieder, H. Rapp, J. Roth, F. Ryter, F. Schneider, G. Siller, P. Smeulders, F. Söldner, E. Speth, A. Stäbler, K. Steuer, O. Vollmer, F. Wagner, *Proceedings of the 12th European Conference on Controlled Fusion and Plasma Physics*, Budapest, Hungary, 1985, edited by L. Póas and A. Montvai (European Physical Society, Budapest, 1985), Vol. I, p. 18.
8. C. M. Surko and R. E. Slusher, Science 221, 817 (1983).
9. S. J. Zweben and R. W. Gould, Nucl. Fusion **23**, 1625 (1983).
10. S. J. Levinson, J. M. Beall, E. J. Powers, and R. D. Bengtson, Nucl. Fusion **24**, 527 (1984).
11. Ch. P. Ritz, Roger D. Bengtson, S. J. Levinson, and E. J. Powers, Phys. Fluids **27**, 2956 (1984).
12. A. J. Wootton, H. Howe, P. H. Edmonds, C. H. Ma, P. K. Mioduszewki, K. Yokoyama, submitted to Nucl. Fusion (1985).
13. D. L. Brower, Private Communication.
14. William L. Rowan, C. C. Klepper, Ch. P. Ritz, Roger D. Bengtson, K. W. Gentle, P. E. Phillips, T. L. Rhodes, B. Richards, and A. J. Wootton, submitted to Nucl. Fusion (1985).
15. B. A. Carreras, P. H. Diamond, M. Murakami, J. L. Dunlap, J. D. Bell, H. R. Hicks, J. A. Holmes, E. A. Lazarus, V. K. Paré, P. Similon, C. E. Thomas, and R. M. Wieland, Phys. Rev. Lett. **50**, 503 (1983).
16. F. Wagner, Private Communication.
17. D. C. Robinson, N. R. Ainsworth, M. W. Alcock, D. Atkinson, P. R. Collins, A. N. Dellis, T. Edlington, A. Ferreira, Q. Gao, T. C. Hender, Z. Ma, A. W. Morris, M. O'Brien, B. Parham, A. C. Riviere, D. F. H. Start, S. Takamura, T. N. Todd, in **Plasma Physics and Controlled Nuclear Fusion Research**, 1984 (IAEA, Vienna, 1985), Vol. I, p. 205.
18. M. L. Sawley, A. Pochelon, and R. Keller, Ref. 7, Vol. I, p. 291.

19. L. Garcia, P. H. Diamond, B. A. Carreras, and J. D. Callen, Phys. Fluids **28**, 2147 (1985).

20. T. S. Hahm, P. H. Diamond, P. W. Terry, L. Garcia, and B. A. Carreras, submitted to Phys. Fluids (1985).

21. C. M. Bishop, P. Kirby, J. W. Connor, R. J. Hastie, J. B. Taylor, Nucl. Fusion **12**, 1579 (1984).

22. G. v. Gierke, M. Keilhacker, R. Bartiromo, G. Becker, H. S. Bosch, A. Eberhagen, G. Fussmann, O. Gehre, J. Gernhardt, E. Glock, O. Gruber, G. Haas, G. Janeschitz, F. Karger, O. Klüber, M. Kornherr, P. B. Kotze, K. Lackner, M. Lenoci, G. Lisitano, H. M. Mayer, K. McCormick, D. Meisel, V. Mertens, E. R. Müller, H. Murmann, H. Niedermeyer, W. Poschenrieder, H. Rapp, F. Ryter, F. Schneider, G. Siller, P. Smeulders, F. Söldner, E. Speth, K. H. Steuer, O. Vollmer, and F. Wagner, Ref. 7, Vol. I, p. 331.

23. W. X. Qu and J. D. Callen, Bull. Am. Phys. Soc. **29**, 1387 (1984).

24. C. Mercier and N. Luc, in **MHD Approach to Confinement in Toroidal Systems**, Commission of the European Communities, Brussels, Rep. EUR-5127e (1974) p. 140.

25. J. W. Connor, R. J. Hastie, and J. B. Taylor, Phys. Rev. Lett. **40**, 396 (1978).

26. T. C. Hender, B. A. Carreras, W. A. Cooper, J. A. Holmes, P. H. Diamond, and P. L. Similon, Phys. Fluids **27**, 1439 (1984).

27. P. H. Diamond, P. L. Similon, T. C. Hender, and B. A. Carreras, Phys. Fluids **28**, 1116 (1985).

28. H. R. Strauss, Phys. Fluids **24**, 2004 (1981).

29. J. W. Connor, R. J. Hastie, T. J. Martin, A. Sykes, M. F. Turner, in **Plasma Physics and Controlled Nuclear Fusion Research** (IAEA, Baltimore, 1982), Vol. III, p. 403.

30. J. F. Drake and T. M. Antonsen, Jr., Phys. Fluids **28**, 544 (1985).

31. P. C. Liewer, J. M. McChesney, S. J. Zweben, and R. W. Gould, Phys. Fluids **29**, 309 (1986).

32. A. Howling, A. Cote, E. J. Doyle, D. E. Evans, and D. C. Robinson, Ref. 7, p. 311.

33. P. H. Rutherford, in **Physics of Plasma Close to Thermonuclear Conditions**, edited by B. Coppi, et. al, (Pergamon Press, New York, 1981), Vol. I, p. 143.

Figure Captions

Fig. 1 Model Divertor Equilibrium Configuration.

Fig. 2 Enhancements of global shear ($\hat{s}$) and the safety factor (q_{MHD}) due to separatrix geometry as functions of flux-surface shape ($\hat{s}_c = 2$ is used).

Fig. 3 Resistive kink stability parameter Δ' as a function of Σ, a current density gradient parameter.

Fig. 4 Reduction of thermal diffusivity, χ_e, due to separatrix geometry as a function of flux-surface shape.

Fig. 5 Reduction of particle diffusivity, D_n, due to separatrix geometry as a function of flux-surface shape.

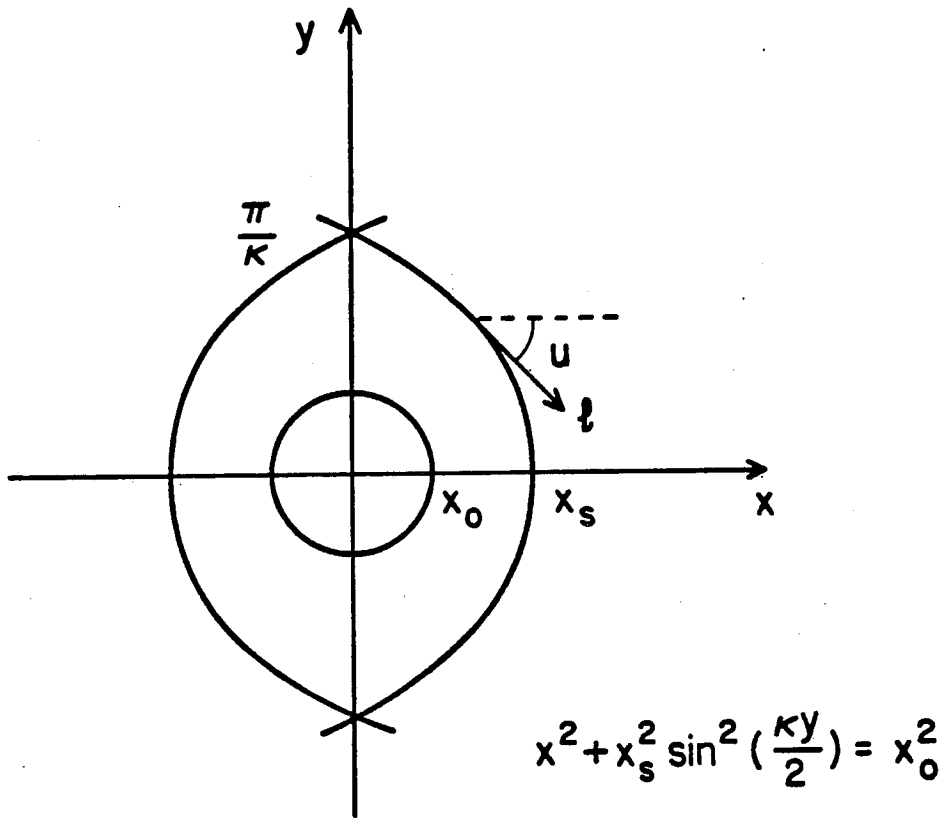

Fig. 1

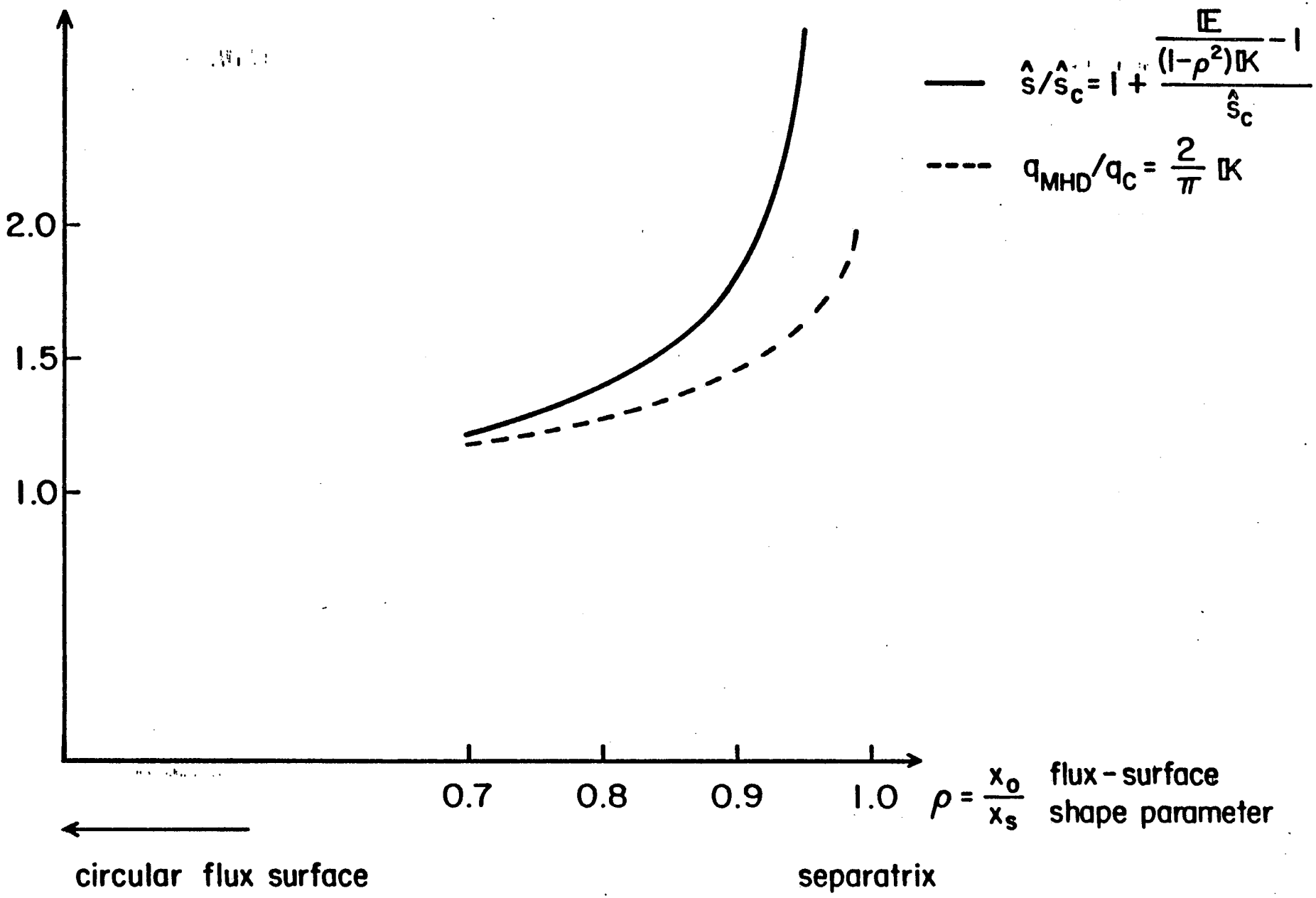
$\hat{s}/\hat{s}_c = 1 + \frac{\mathbb{E}}{(1-\rho^2)\mathbb{K}} - 1$
$q_{MHD}/q_c = \frac{2}{\pi}\mathbb{K}$
2.0
1.5
1.0
0.7
0.8
0.9
1.0
$\rho = \frac{x_0}{x_s}$ flux-surface shape parameter
circular flux surface
separatrix

Fig. 2

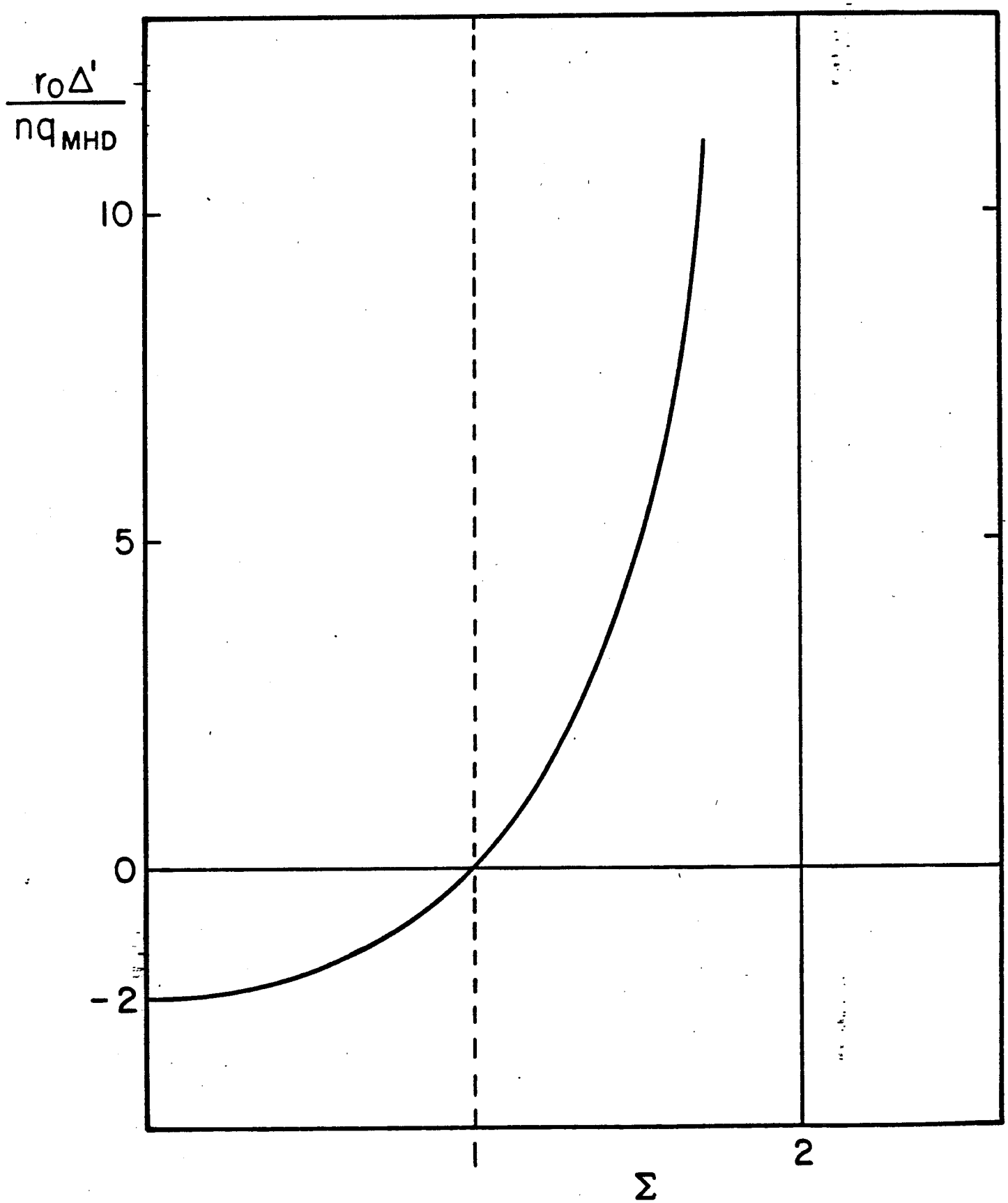

Fig. 3

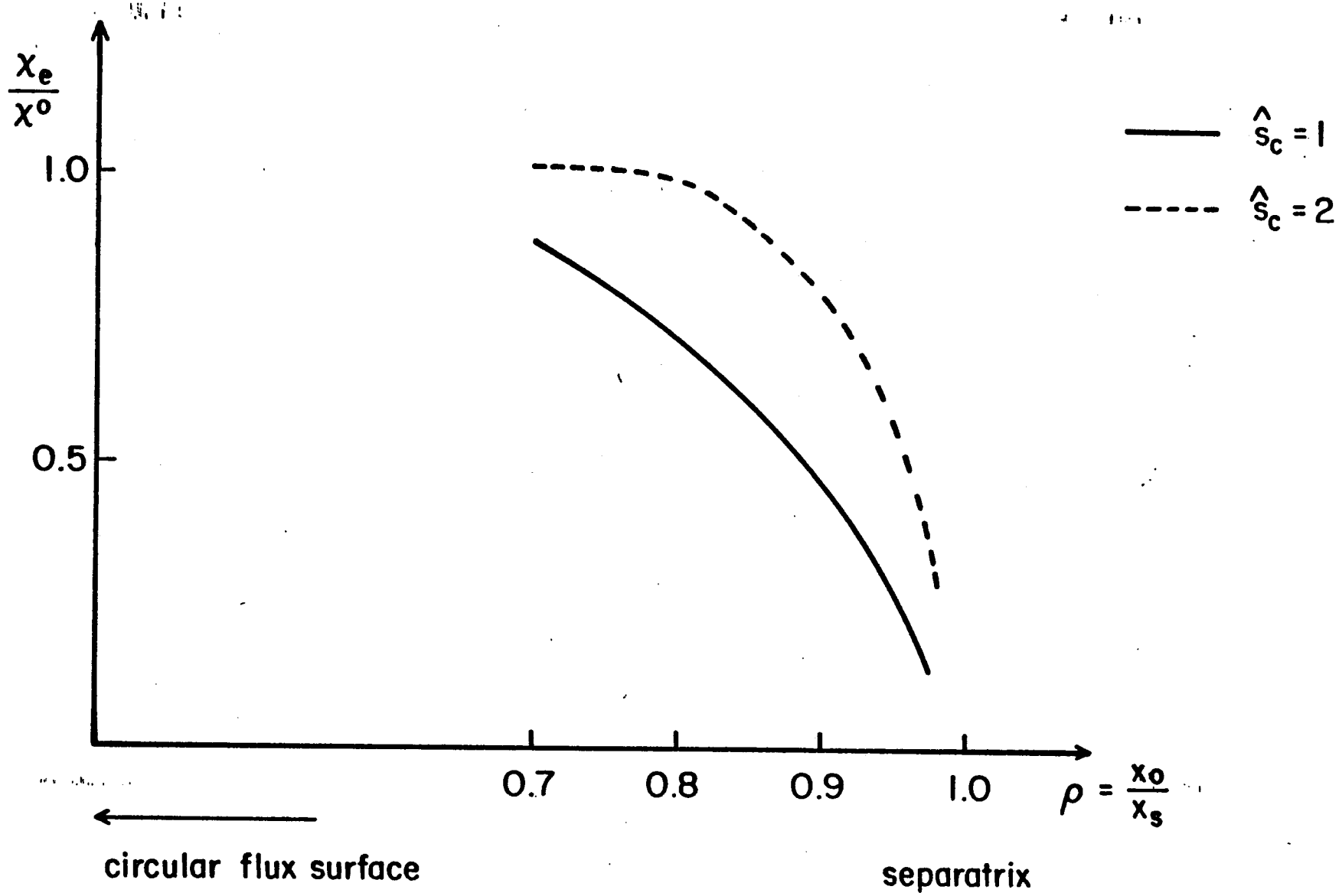
$\frac{\chi_e}{\chi^o}$
1.0
0.5
$\hat{s}_c = 1$
$\hat{s}_c = 2$
0.7
0.8
0.9
1.0
$\rho = \frac{x_o}{x_s}$
circular flux surface
separatrix

Fig. 4

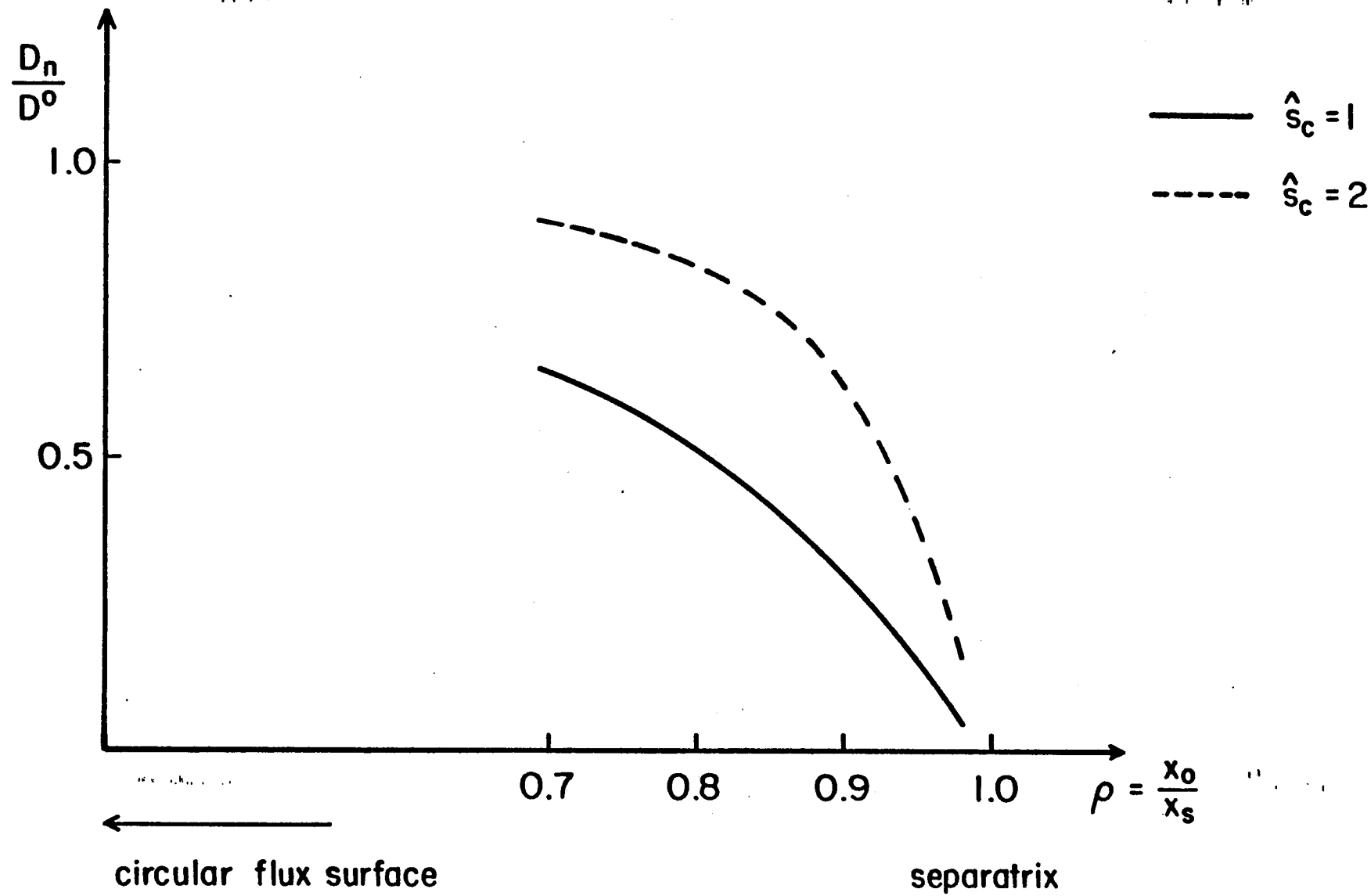
$\frac{D_n}{D^o}$
1.0
0.5
$\hat{s}_c = 1$
$\hat{s}_c = 2$
0.7
0.8
0.9
1.0
$\rho = \frac{x_o}{x_s}$
circular flux surface
separatrix

Fig. 5